analytical chemistry

Article

pubs.acs.org/ac

Integrated Nanozymes with Nanoscale Proximity for in Vivo Neurochemical Monitoring in Living Brains

Hanjun Cheng,[†,∥] Lei Zhang,[†] Jian He,[‡] Wenjing Guo,[†] Zhengyang Zhou,[*,‡] Xuejin Zhang,[*,†] Shuming Nie,[*,†,§] and Hui Wei[*,†,∥]

[†]College of Engineering and Applied Sciences, Nanjing National Laboratory of Microstructures, Nanjing University, Nanjing, Jiangsu 210093, China

[‡]Department of Radiology, Nanjing Drum Tower Hospital, The Affiliated Hospital of Nanjing University Medical School, Nanjing, Jiangsu 210008, China

[§]Department of Biomedical Engineering, Emory University, Atlanta, Georgia 30322, United States

[∥]Collaborative Innovation Center of Chemistry for Life Sciences, State Key Laboratory of Analytical Chemistry for Life Science, Nanjing University, Nanjing, Jiangsu 210093, China

Supporting Information

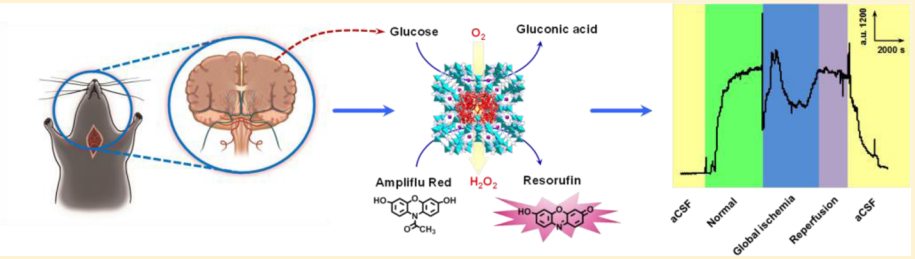

ABSTRACT: Nanozymes, the nanostructures with enzymatic activities, have attracted considerable attention because, in comparison with natural enzymes, they offer the possibility of lowered cost, improved stability, and excellent recyclability. However, the specificity and catalytic activity of current nanozymes are still far lower than that of their natural counterparts, which in turn has limited their use such as in bioanalysis. To address these challenges, herein we report the design and development of integrated nanozymes (INAzymes) by simultaneously embedding two cascade catalysts (i.e., a molecular catalyst hemin and a natural enzyme glucose oxidase, GOx) inside zeolitic imidazolate framework (ZIF-8) nanostructures. Such integrated design endowed the INAzymes with major advantage in improved catalytic efficiency as the first enzymatic reaction occurred in close (nanoscale) proximity to the second enzyme, so products of the first reaction can be used immediately as substrates for the second reaction, thus overcoming the problems of diffusion-limited kinetics and product instability. The considerable high catalytic activity and stability enabled the INAzymes to efficiently draw a colorimetric detection of glucose with good sensitivity and selectivity. When facilitated with in vivo microdialysis, the INAzyme was successfully used for facile colorimetric visualization of cerebral glucose in the brain of living rats. Moreover, when further combined with microfluidic technology, an integrative INAzyme-based online in vivo analytical platform was constructed. The promising application of the platform was successfully illustrated by continuously monitoring the dynamic changes of striatum glucose in living rats' brain following ischemia/reperfusion. This study developed a useful approach to not only functional nanomaterial design but also advanced platforms developments for diverse targets monitoring.

Nanozymes, the nanostructures with enzymatic activities, have attracted particular attention as emerging natural enzyme mimics.[1,2] Because of their unique characteristics relative to natural enzymes and even conventional artificial enzymes, nanozymes have been extensively explored for wide applications, such as in bioanalysis,[3−24] bioimaging,[25,26] and biomedicine.[27−31] For instance, researchers have recently achieved the selective glucose detection in serum by exploring the catalase-mimicking activity of cerium oxide nanoparticles.[5]

Despite the substantial progress, the specificity and catalytic activity of currently developed nanozymes are still far lower than that of natural enzymes.[1,2,32−39] These shortcomings have in turn impeded the use of nanozymes, such as in bioanalysis (especially in in vivo analysis). Therefore, great efforts have been devoted to tackling these unmet challenges. The selectivity challenge could be partially overcome by combining a nanozyme with a natural enzyme, as demonstrated in our previous study.[4] In that case, iron oxide nanoparticle-based peroxidase mimic was combined with natural glucose oxidase (GOx) for colorimetric detection of glucose. However, the

Received: March 11, 2016
Accepted: April 12, 2016

DOI: 10.1021/acs.analchem.6b00975
Anal. Chem. XXXX, XXX, XXX−XXX

nanozyme and natural enzyme worked separately to catalyze single isolated reactions rather than coupled tandem reactions. Such a separation would inevitably lead to lowered local concentration of the catalysts (i.e., nanozymes and natural enzymes) and their substrates as well as potential decomposition of the intermediates (e.g., H_2O_2), therefore resulting in limited overall efficiency of the enzymatic reactions.

Biological systems, on the other hand, use multiple enzymes confined within subcellular compartments as sophisticated enzyme assemblies for highly complex cascade catalytic reactions.[40−42] Such confinement would significantly enhance the overall efficiency of enzymatic reactions by improving the enzymes' stability, reducing the diffusion barrier, and minimizing the decomposition of highly active intermediates due to the "nanoscale proximity effects". Inspired by this promising phenomenon, here we reason that a highly efficient "integrated nanozyme (INAzyme)" could be developed by combining natural enzymes and nanozymes within confined space, which has not been achieved yet due to several challenges. For instance, most of the commonly employed methods require high temperature and/or organic solvents, which are not compatible with bioactive molecules.[38] Post-modification (such as covalent conjugation of enzymes) is also usually needed, which inevitably affects the enzyme activity.[28,43]

To tackle these challenges, here we report a biocompatible strategy to prepare high-performance INAzymes by adaptively coassembling molecular catalysts (i.e., hemin) and natural enzymes (i.e., GOx) within a nanoscaled metal−organic framework (MOF) (Figure 1). We have chosen zeolitic imidazolate framework (ZIF-8) as a model of nanoscaled MOF host instead of other hosts owing to its biocompatible synthesis, good crystallinity, and high surface-area-to-volume ratio.[44−49] We have successfully obtained INAzymes (i.e., GOx/hemin@ZIF-8) with various merits such as remarkably enhanced catalytic activity and excellent stability due to the nanoscale proximity effects. Notably, our strategy was applicable to others enzymes (i.e., LOx/hemin@ZIF-8, LOx is lactate oxidase) and multiple biocatalyst systems (i.e., invertase/GOx/hemin@ZIF-8), which also exhibited enhanced catalytic activities and improved stability. To demonstrate the promising application of the designed INAzymes for in vivo analysis, GOx/hemin@ZIF-8 was used for selective and sensitive detection of neurochemicals in living brains. Cerebral glucose was chosen as a model neurochemical because it is the most important energy source in the central nervous system. Furthermore, when facilitated by microfluidic technology, an integrative analytical platform was constructed with GOx/hemin@ZIF-8 for in vivo real-time monitoring the dynamic changes of stratum glucose in living brains following ischemia/reperfusion (Figure S1).

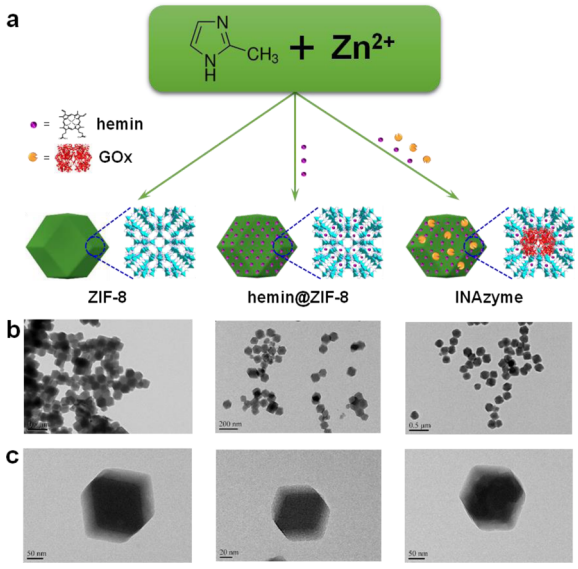

Figure 1. Biocompatible synthesis and characterization of nanoscaled ZIF-8 and ZIF-8-based nanozymes. (a) Schematic illustration of the biocompatible one-step synthetic approaches to nanoscaled ZIF-8 and ZIF-8-based nanozymes in aqueous solution at room temperature. ZIF-8 was prepared by assembling 2-methylimidazole and zinc acetate, while hemin@ZIF-8 as peroxidase mimic and GOx/hemin@ZIF-8 as the INAzyme were prepared by encapsulating hemin and GOx/hemin within ZIF-8 frameworks in a one-step protocol, respectively. The enlarged pictures at the bottom of panel a schematically show the models of ZIF-8 and ZIF-8-based nanozymes. For clarity, the models are not drawn to scale. (b and c) Transmission electron microscopy (TEM) images of ZIF-8 and ZIF-8-based nanozymes at low magnification (b) and high magnification (c).

EXPERIMENTAL SECTION

Synthesis of ZIF-8 and ZIF-8-Based Nanocomposites. (a) ZIF-8: ZIF-8 was synthesized according to the previous literatures with several modifications.[50] Briefly, 2 mL of 0.50 M zinc acetate aqueous solution was quickly poured into 2 mL of 2.0 M 2-methylimidazole aqueous solution. The mixture was magnetically stirred at room temperature overnight, and the obtained white precipitates were centrifuged and washed by anhydrous ethanol and deionized water for several times. Finally, the product was dried at 80 °C under in vacuo for 12 h. (b) Hemin@ZIF-8: The hemin@ZIF-8 nanozyme was prepared by adaptively incorporating guest molecule hemin into the ZIF-8 framework during the self-assembly of Zn^{2+} and 2-methylimidazole. Typically, 20 μL of 20 mM hemin in DMSO was added into 2 mL of 2.0 M 2-methylimidazole aqueous solution under magnetic stirring to get a homogeneous mixture. Then 2 mL of 0.50 M zinc acetate aqueous solution was added. The resultant mixture was stirred at room temperature overnight. The obtained light green precipitates were centrifuged and washed by deionized water for several times. (c) GOx@ZIF-8: The GOx@ZIF-8 was prepared using 30 μL of 20 mg/mL GOx aqueous solution instead of hemin, under conditions otherwise identical to those used for preparing hemin@ZIF-8. (d) GOx/hemin@ZIF-8: The GOx/hemin@ZIF-8 was prepared using 20 μL of 20 mM hemin and 30 μL of 20 mg/mL GOx instead of hemin, under conditions otherwise identical to those used for preparing hemin@ZIF-8. (e) GOx−FITC/hemin@ZIF-8: The GOx−FITC/hemin@ZIF-8 was prepared using 20 μL of 20 mM hemin and 30 μL of 2 mg/mL GOx-FITC instead of hemin, under conditions otherwise identical to those used for preparing hemin@ZIF-8.

Evaluation of the Peroxidase-Mimicking Activity of Hemin@ZIF-8 Nanozyme. The peroxidase-mimicking activity of the as-prepared hemin@ZIF-8 was assessed by using the peroxidase chromogenic substrate 2,2′-azino-bis(3-ethylbenzothiazoline-6-sulphonic acid) (ABTS) as the reporting molecule. In a typical experiment, 5 μL of hemin@ZIF-8 suspension (20 mg/mL) was added into 0.10 M Tris−HCl buffer (pH 7.0) containing H_2O_2 (2 μL, 100 mM) and ABTS (40 μL, 50 mM). The final volume of the mixture was adjusted to 1 mL with 0.10 M Tris−HCl buffer (pH 7.0), and the mixed solution was then

DOI: 10.1021/acs.analchem.6b00975
Anal. Chem. XXXX, XXX, XXX−XXX

incubated in a 37 °C water bath for 20 min. After removal of hemin@ZIF-8 nanozymes by centrifugation, the resulting supernatant solution was used for colorimetric visualization through photographing with a digital camera or for adsorption spectroscopy measurement on a UV−vis spectrophotometer.

In Vitro Measurement of Glucose. The cascade enzymatic activity of the INAzyme was assessed by oxidation of glucose and the peroxidase chromogenic substrate ABTS. In a typical experiment, 10 μL of the INAzyme (20 mg/mL) was added into 0.10 M Tris−HCl buffer (pH 7.0) containing glucose (20 μL, 10 mM) and ABTS (40 μL, 50 mM). The final volume of the mixture was adjusted to 1 mL with 0.10 M Tris−HCl buffer (pH 7.0), and the mixed solution was then incubated in a 37 °C water bath for 1 h. After removal of the INAzyme by centrifugation, the resulting supernatant solution was used for colorimetric visualization through photographing with a digital camera or for adsorption spectroscopy measurement on a UV−vis spectrophotometer.

For colorimetric visualization and spectrometric measurement of glucose, different concentrations of glucose in artificial cerebrospinal fluid (aCSF) was added into 0.10 M Tris−HCl buffer (pH 7.0) containing INAzymes (200 μg/mL) and ABTS (2 mM), and the final volume was adjusted to 1 mL. After thorough mixing, the resulting solution was incubated at 37 °C for 1 h. After removal of the INAzymes by centrifugation, the mixtures were then photographed with a digital camera and the corresponding absorption spectra were recorded on a UV−vis spectrophotometer.

Off-Line in Vivo Measurement of Cerebral Glucose. For the measurement of glucose in the microdialysate sampled from the striatum of living rat brain, 200 μL of the collected brain microdialysate, 8 μL of INAzyme (20 mg/mL), and 32 μL of ABTS solution (50 mM) were added into 560 μL of 0.10 M Tris−HCl buffer (pH 7.0). The resulting solution was thoroughly mixed and then incubated at 37 °C for 1 h. Then, the INAzymes were removed upon centrifugation and the supernatant solution was photographed and measured by UV−vis spectroscopy.

INAzyme-Based Integrative Online Sensing Platform. As illustrated in Figure S1, the INAzyme-based integrative fluorescent sensing platform for continuously monitoring neurochemicals in the brain of living animals (cerebral glucose in living rats as an example in the current study) was constructed by rationally coupling in vivo microdialysis with an I-shaped microfluidic chip and a home-built fluorescent detection system. The INAzymes were immobilized within the microchannel of the microfluidic chip. The fluorescent detection of glucose was achieved as follows: Brain microdialysates were continuously sampled from the rat brain via pump 2 (CMA 401, CMA Microdialysis AB, Stockholm, Sweden) with aCSF as the perfusion solution at 1 μL/min. The peroxidase substrate Ampliflu Red solution (369 μM in 0.10 M Tris−HCl buffer (pH 6.5)) was supplied with pump 1 at 1 μL/min. The microdialysates and the Ampliflu Red solution were then mixed online through a T-joint and subsequently delivered into the INAzyme-immobilized microchip, where they reacted with the confined INAzymes via the cascade enzymatic reactions to produce fluorescent resorufin for detection. The formed resorufin was excited with a 532 nm laser, which was focused onto the position with a distance of 2 mm away from the outlet of the microchip. The emission spectra from 560 to 620 nm were consecutively collected with a time interval of 5 s. The fluorescence intensity at 585 nm was used for glucose monitoring.

Living Brain Ischemia and Reperfusion Surgery. The animal studies were approved by the Committee for Experimental Animals Welfare and Ethics of Nanjing Drum Tower Hospital, the Affiliated Hospital of Nanjing University Medical School. Adult male Sprague−Dawley rats (350−400 g) were purchased from Jiesijie Laboratory Animal Co. (Shanghai, China). Rats' surgeries were performed as reported previously.[51−54] Briefly, the rats were anesthetized with chloral hydrate (345 mg/kg, ip) and positioned onto a stereotaxic frame. A microdialysis guide cannula (BAS/MD-2250, BAS) was implanted into the striatum following standard stereotaxic procedures. The guide cannula was kept in place with three skull screws and dental cement. A stainless steel dummy blocker was inserted into the guide cannula and fixed until the insertion of a microdialysis probe. Throughout the surgery, the body temperature of the rats was maintained at 37 °C with a heating pad. After the rats were allowed to recover for at least 24 h, a microdialysis probe with a diameter of 0.24 mm (BAS) was implanted into the rat striatum. aCSF solution was then continuously perfused for equilibration.

Note that there were slight differences in rats' surgeries between off-line and online detection of cerebral glucose. For off-line detection of cerebral glucose, a microdialysis probe with a length of 2 mm was positioned at AP = 0 mm, L = 3 mm from bregma, V = 3.5 mm from dura. The microdialysate was thus collected with aCSF solution perfused at 2 μL min^{-1} for analysis. However, for online detection of cerebral glucose, a microdialysis probe with a length of 4 mm was implanted with the position at AP = 0 mm, L = 3.5 mm from bregma, V = 2.5 mm from dura. The aCSF solution was perfused at 1 μL min^{-1}.

Surgeries for the global cerebral ischemia/reperfusion were performed with a method described previously.[53] Briefly, through a midline cervical incision, both common carotid arteries were exposed and isolated from surrounding connective tissue. Note, special care was needed to avoid damaging the vagus or the sympathetic nerves running close by. Global ischemia and reperfusion were induced by first occluding both carotid arteries with nontraumatic arterial clips for ischemia and then removing the clips for reperfusion. Throughout the operation, the body temperature of the rats was maintained at 37 °C using a heating pad.

RESULTS AND DISCUSSION

Design and Synthesis of ZIF-8-Based Nanozymes. The design strategy for ZIF-8-based nanozymes is shown in Figure 1a. ZIF-8, constructed from zinc ions and 2-methylimidazole, was chosen as the host matrix because of its facile synthesis, good crystallinity, and high surface-area-to-volume ratio.[44,55] To preserve the bioactivities of encapsulated guest molecules (i.e., GOx and hemin), a biocompatible synthetic protocol was adopted. The hemin@ZIF-8 and the INAzyme were synthesized by simultaneously incorporating hemin and GOx/hemin within nanoscaled ZIF-8 at room temperature in aqueous solution, respectively. Compared with ZIF-8 of rhombic dodecahedral shape, the morphology evolution of hemin@ZIF-8 and the INAzyme to less regular shapes implied the guest molecules encapsulation within ZIF-8 hosts (Figure 1, parts b and c). ZIF-8, hemin@ZIF-8, and the INAzyme had average sizes of ca. 210, 100, and 190 nm, respectively, which is critical for biomedical applications. The size variations between ZIF-8 and the nanozymes also indicated the guest molecules

DOI: 10.1021/acs.analchem.6b00975
Anal. Chem. XXXX, XXX, XXX−XXX

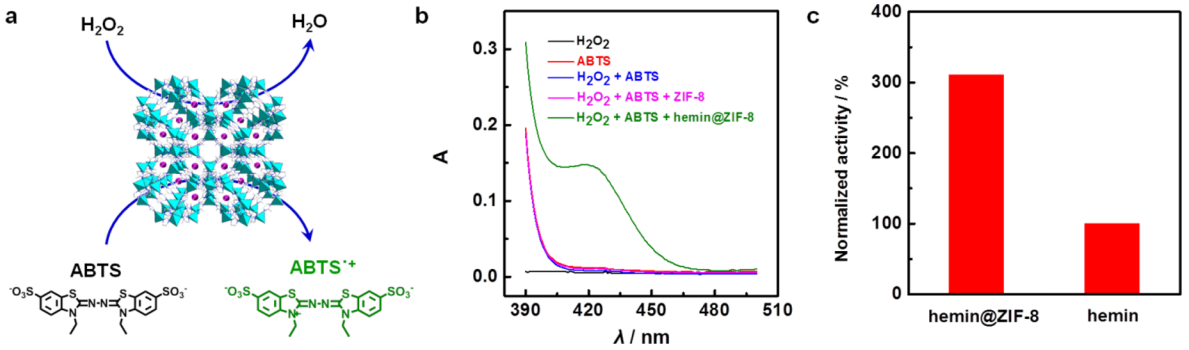

Figure 2. Hemin@ZIF-8 nanozyme as enhanced peroxidase mimic. (a) Schematic illustration of hemin@ZIF-8-catalyzed oxidation of ABTS with H_2O_2 to produce green-colored ABTS$^{\bullet+}$. (b) UV−vis absorption spectra of H_2O_2 (black curve), ABTS (red curve), H_2O_2 + ABTS (blue curve), H_2O_2 + ABTS + ZIF-8 (pink curve), and H_2O_2 + ABTS + hemin@ZIF-8 (green curve) in 0.10 M Tris−HCl buffer (pH 7.0), respectively. (c) Normalized peroxidase-mimicking activities of hemin@ZIF-8 and hemin, showing a more than 300% enhancement for hemin@ZIF-8 when compared with hemin in aqueous solution.

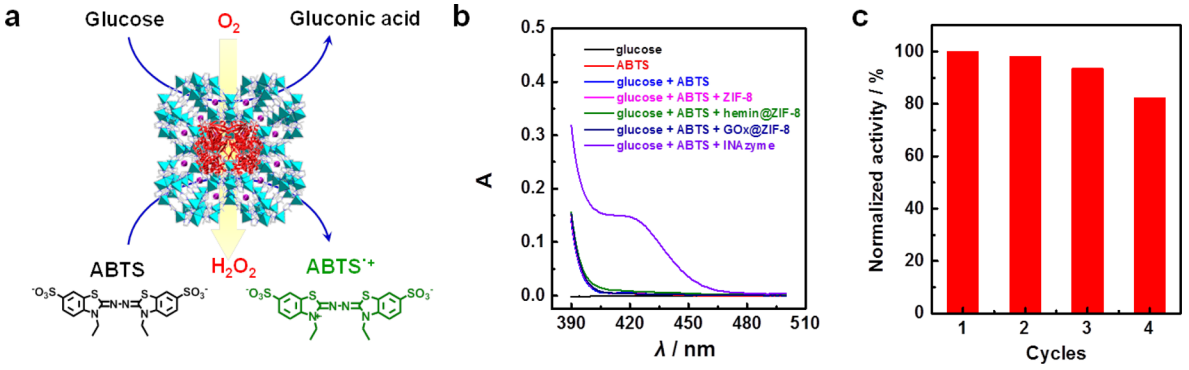

Figure 3. GOx/hemin@ZIF-8 as the INAzyme. (a) Schematic illustration of the INAzyme-catalyzed cascade oxidation of glucose and ABTS to produce green-colored ABTS$^{\bullet+}$. (b) UV−vis absorption spectra of glucose (black curve), ABTS (red curve), glucose + ABTS (blue curve), glucose + ABTS + ZIF-8 (pink curve), glucose + ABTS + hemin@ZIF-8 (green curve), glucose + ABTS + GOx@ZIF-8 (navy curve), and glucose + ABTS + GOx/hemin@ZIF-8 (violet curve) in 0.10 M Tris−HCl buffer (pH 7.0), respectively. (c) Normalized catalytic activities of the INAzyme after recycling.

encapsulation. Interestingly, the X-ray diffraction (XRD) patterns of the two nanozymes were almost identical to both the simulated and measured patterns of ZIF-8, indicating that the encapsulation had negligible effects on the phase of ZIF-8 hosts (Figure S2).

To further validate the successful encapsulation of hemin and GOx/hemin within the nanozymes, element mapping was performed. The uniform distribution of Fe, the characteristic element of hemin, through both nanozymes demonstrated the successful encapsulation of hemin (Figure S3). As a comparison, no Fe was detected for ZIF-8 alone. Though S is peculiar to the encapsulated GOx, its content is low. Therefore, the encapsulation of GOx was validated by fluorescence labeling. GOx was conjugated with fluorescein isothiocyanate (FITC), and the conjugate was used instead of GOx to prepare GOx−FITC/hemin@ZIF-8 nanoparticles. Bright lime green fluorescence from the as-prepared nanoparticles was clearly observed when they were excited at 436 nm, indicating the successful encapsulation of GOx (Figure S4). These results demonstrated that both hemin and GOx could be conveniently incorporated into ZIF-8 during the framework formation through self-assembly chemistry to form the nanozymes, whose enzyme-mimicking activities and applications for in vivo measurements are investigated below.

Hemin@ZIF-8 as Enhanced Peroxidase Mimic. The peroxidase-like activity of hemin@ZIF-8 nanozyme was evaluated through the catalytic oxidation of ABTS (a peroxidase chromogenic substrate) with H_2O_2 (Figure 2a). The introduction of hemin@ZIF-8 nanozymes into Tris−HCl buffer containing H_2O_2 and ABTS resulted in an immediate color change from colorless to green, demonstrating the nanozyme-catalyzed oxidation of ABTS to its product ABTS$^{\bullet+}$ (Figures 2b and S6). As a comparison, H_2O_2, ABTS, or H_2O_2/ABTS exhibited no color changes, indicating that no oxidation reaction occurred. More, the substitution of hemin@ZIF-8 with ZIF-8 did not produce any color changes either, suggesting that the peroxidase-like activity of hemin@ZIF-8 nanozyme originated from the encapsulated hemin while ZIF-8 mainly served as the encapsulating matrix.

To further assess the remarkable peroxidase-like activity of hemin@ZIF-8 nanozyme, the following control experiments were performed. When the same amount of free hemin in aqueous solution was used to catalyze the oxidation of ABTS, green-colored ABTS$^{\bullet+}$ was slowly produced in contrast to the instant color change catalyzed by hemin@ZIF-8. The quantitative analysis of the initial reaction rates revealed that a more than 300% enhancement of the peroxidase-like activity for hemin@ZIF-8 was obtained when compared with free hemin (Figures 2c and S7). The remarkably enhanced peroxidase-like activity of hemin@ZIF-8 could be attributed to several factors, including the high surface-area-to-volume ratio and enriching effects of ZIF-8 frameworks and, most

DOI: 10.1021/acs.analchem.6b00975
Anal. Chem. XXXX, XXX, XXX−XXX

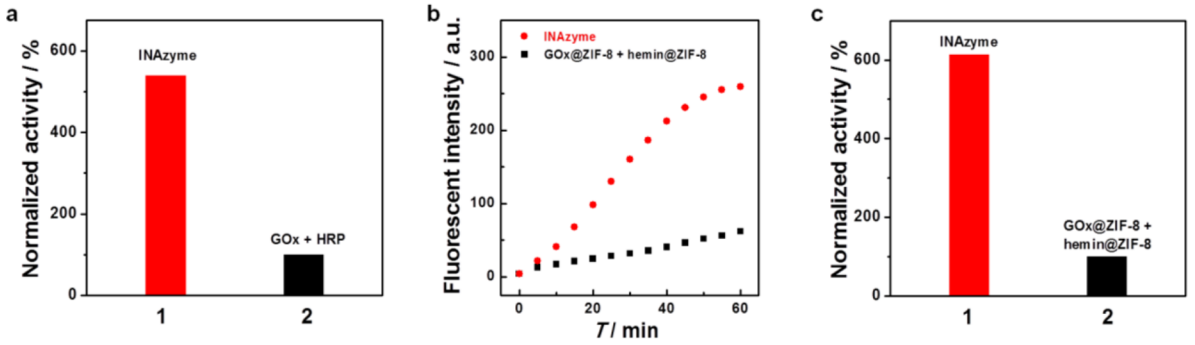

Figure 4. Nanoscale proximity effects on the catalytic activities of the INAzyme. (a) Normalized catalytic activities of the INAzyme (1) and free GOx/HRP (2) evaluated after 80 °C treatment, showing a more than 500% enhancement for the INAzyme when compared with free GOx/HRP. (b) Kinetic plots of time-dependent fluorescent intensity of 0.10 M Tris−HCl buffer (pH 7.0) containing 1 mM glucose, 155 μM Ampliflu Red, and 200 μg/mL of the INAzyme (●) or the mixture of 200 μg/mL of hemin@ZIF-8 and 200 μg/mL of GOx@ZIF-8 (■). (c) Normalized cascade catalytic activity of the INAzyme (1), and the mixture of hemin@ZIF-8 and GOx@ZIF-8 (2), showing a more than 600% enhancement for the INAzyme when compared with the mixture of hemin@ZIF-8 and GOx@ZIF-8.

importantly, the well-preserved hemin monomers within ZIF-8 frameworks. In contrast, free hemin forms dimer and multimer aggregates in aqueous solution, which contribute poorly to its peroxidase-like activity.[56] To further demonstrate our hypothesis, the corresponding absorption spectra were recorded. The hemin@ZIF-8 exhibited a sharp Soret band at 398 nm, the characteristics of the monomer form of hemin, which was similar to the Soret band at 405 nm from hemin in DMSO (Figure S8). The slightly blue-shifted Soret band of hemin@ZIF-8 indicated the interactions between confined hemin and ZIF-8 framework. Hemin in aqueous solution, by contrast, exhibited a significantly broadened Soret band, revealing the presence of severe hemin aggregates. The spectroscopic studies indicated that ZIF-8 frameworks well-maintained the monomer form of encapsulated hemin, and thus endowed hemin@ZIF-8 with excellent peroxidase-mimicking activity.

The recyclability of hemin@ZIF-8 was also investigated, showing hemin@ZIF-8 retained more than 90% of its initial catalytic activity after recycling (Figure S9). Thus, these results demonstrated that, by encapsulating catalytic guests within ZIF-8 frameworks, highly active nanozymes could be rationally designed and facilely synthesized.

GOx/Hemin@ZIF-8 as the High-Performance INAzyme. After evaluating the peroxidase-like activity of hemin@ZIF-8 nanozyme, the performance of GOx/hemin@ZIF-8 as the INAzyme for cascade reactions was examined (Figure 3). As shown in Figure 3a, by coassembling GOx/hemin within ZIF-8 frameworks, the designed INAzyme would enable the following cascade reactions. First, the GOx catalyzed the oxidation of glucose with dioxygen to locally produce H_2O_2. Subsequently, the adjacent hemin catalyzed the oxidation of a peroxidase substrate (here ABTS as the colorimetric substrate) with the in situ formed H_2O_2 to generate detection signals (here the colored $ABTS^{\bullet+}$). When the INAzyme was added into the solution containing glucose and ABTS, distinguishable green color emerged after incubation at 37 °C, suggesting that cascade biocatalysis proceeded as designed (Figure S11). When ZIF-8, hemin@ZIF-8, or GOx@ZIF-8 was tested, however, no color change was observed (Figures 3b and S11). These results substantially demonstrated the necessity of integrating both GOx and hemin within ZIF-8 framework for the designed cascade reactions. Such integration would endow the INAzyme with multiple unique merits, such as recyclability, prolonged shelf-time, improved stability, and enhanced activity.

Similar to hemin@ZIF-8, the INAzyme was also recyclable. The INAzyme retained more than 80% of its initial activity after recycling (Figure 3c). In addition, the INAzyme exhibited good long-term storage stability. Compared with fresh INAzyme, as high as 85% activity was retained after 2 months of storage at 4 °C (Figure S12). The potential leakage of the encapsulated guests within ZIF-8 was also investigated. As shown in Figure S13, the potentially leaked hemin and GOx were negligible, suggesting that both the guests were tightly encapsulated with the ZIF-8 frameworks. Overall, the INAzymes showed excellent recyclability as well as very good stability and robust activity over an extended period.

Nanoscale Proximity Effects on the Catalytic Activities of the INAzyme. The confinement of cascade catalysts within a nanoscaled space would not only significantly improve the catalysts' stability but also effectively promote the complementary reactions by reducing the diffusion barrier and minimizing the decomposition of highly active intermediates.[41,42]

The potential nanoscale proximity effects on the catalytic activities of the INAzymes were then investigated. As demonstrated above, the INAzymes exhibited long-term stability, which was probably due to the protection of the encapsulated guests from chemical and biological degradation. Then, the thermal stability of the INAzyme was studied. After treating the INAzymes (or the mixture of free GOx and HRP) at 80 °C, the cascade reactions were carried out with the thermally treated catalysts. As shown in Figure 4a, the INAzyme showed a more than 500% enhancement in catalytic activity relative to free GOx/HRP, indicating that the INAzyme also exhibited prominent thermal stability.

To understand the roles of diffusion barrier in the enhanced catalytic activity of the INAzymes, the following comparisons were carried out. To control the diffusion distances between hemin and GOx, they were intentionally separated as GOx@ZIF-8 and hemin@ZIF-8. Then the mixtures of GOx@ZIF-8 and hemin@ZIF-8 were used for the cascade reactions. As shown in Figure 4b, the INAzyme exhibited much faster catalysis toward the cascade reactions when compared with the mixture. The quantitative analysis showed a more than 600% enhancement in catalytic activity for the INAzymes when compared with the mixture of hemin@ZIF-8 and GOx@ZIF-8 (Figure 4c). For the INAzymes, since hemin and GOx were assembled together within the same ZIF-8 matrixes, the in situ

DOI: 10.1021/acs.analchem.6b00975
Anal. Chem. XXXX, XXX, XXX−XXX

formed H_2O_2 would readily interact with the adjacent hemin and the substrate (Ampliflu Red). For the mixture, however, the formed H_2O_2 had to diffuse out from GOx@ZIF-8 into hemin@ZIF-8 to interact with the hemin and the substrate. Such long diffusion distance dramatically lowered the cascade reaction efficiency. The H_2O_2 may also be decomposed during the diffusion, which would further compromise the catalytic efficiency.

More interestingly, our strategy is general as its versatility can be readily extended to other enzymes and multiple biocatalyst systems, which also exhibited interesting nanoscale proximity effects (Figures S15 and S16).

Off-Line Detection of Cerebral Glucose in Living Brains. The supreme catalytic efficiency of the designed INAzyme essentially enabled it for in vivo bioanalysis. Here cerebral glucose was used as an example to interrogate the INAzyme's analytical performance. As shown in Figure S17, different concentrations of glucose displayed a clear color gradient, suggesting that the presence of glucose and its concentration could be readily visualized with naked eyes. Moreover, the ΔA_{421} of $ABTS^{\bullet+}$ showed a linear increase for glucose from 0 to 250 μM ($\Delta A_{421} = 0.00138 + 0.00505C_{glucose}/\mu M$, $R^2 = 0.96$). This dynamic linear range covers the physiological levels of microdialyzed glucose, thus enabling the INAzymes for the in vivo measurements of glucose in living brains. Note, a detection limit of 1.7 μM was achieved, which was nearly 30-fold lower than our previous result.[4] The improved sensitivity of such INAzyme-based measurement should be ascribed to the enhanced activity of the INAzyme as well as the tandem reactions, which minimized the decomposition and loss of H_2O_2.

Since the microdialysate was directly used for in vivo glucose determination without sample separation and pretreatment (Figure 5a), it is essential to evaluate the selectivity of the established colorimetric assay. Therefore, the key interfering species coexisting in brains were examined, including acrobatic acid (AA), lactate, dopamine (DA), 3,4-dihydroxyphenylacetic acid (DOPAC), uric acid (UA), and 5-hydroxytryptamine (5-HT). Fortunately, none of them at their physiological levels exhibited interference for the glucose detection (Figure S18).

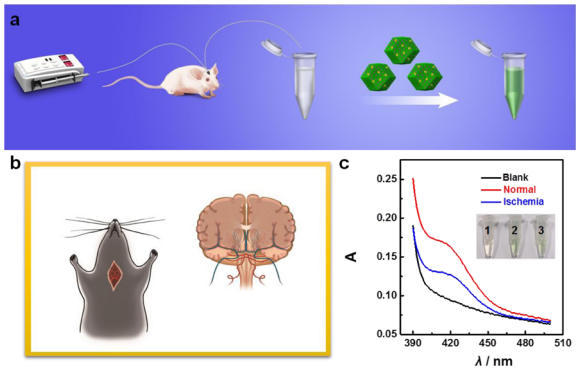

Figure 5. Off-line measurements of cerebral glucose with the INAzyme. (a) Schematic illustration of off-line measuring glucose in the brain of living rats via the INAzyme-catalyzed cascade reactions, which produced green-colored $ABTS^{\bullet+}$ for signaling. (b) Schematic illustration of the global cerebral ischemia. (c) Typical UV−vis absorption spectra and corresponding photographs (inset) of aCSF (1, black curve), microdialysate obtained from rats under normal conditions (2, red curve), and microdialysate obtained from rats subjected to ischemia for 2 h (3, blue curve), respectively.

The excellent selectivity, suitable dynamic range, and high sensitivity of the colorimetric assay validated the INAzyme for measurement of cerebral glucose in living rats.

For off-line measurements of cerebral glucose changes in living rats, the microdialyzed samples were collected before and after global cerebral ischemia (Figure 5, parts a and b). The INAzyme and ABTS were then directly added into the collected microdialysate to produce green color for measurement. As shown in Figure 5c, the microdialysate led to an apparent green color and an absorption peak at 421 nm, whereas the aCSF remained colorless and no characteristic absorption was observed. After the rat was administrated with global cerebral ischemia for 2 h, the collected microdialysate resulted in much weaker signals (both weaker green color and lower absorption) when compared with the results under normal conditions (Figure 5c). Quantitative analysis showed that the basal level of glucose in the microdialysate was 258.0 ± 20.6 μM ($n = 3$) and it decreased to 130.7 ± 10.4 μM ($n = 3$) after global ischemia. The lowered glucose levels following the global ischemia were due to the blockage of cerebral blood flow, which in turn increased the demand of metabolism consumption and diminished respiration.[57] These results demonstrate that with the INAzyme-based colorimetric assay the cerebral glucose under both physiological and pathological processes could be easily visualized by naked eyes or quantified by spectroscopy.

Continuously Online Monitoring Cerebral Glucose with the INAzyme. Though the INAzyme enabled the effective measurement of cerebral glucose in living rats, the above off-line colorimetric assay still suffered from a poor temporal resolution due to the long sample collection time. As a consequence, such a method is still far from the practical needs for continuously in vivo monitoring neurochemicals in living animals, which is of significant therapeutic and scientific importance. For this purpose, microfluidic technology was introduced and well coupled with in vivo microdialysis technology and a fluorescent microscope to form an integrative sensing platform (Figure S1). The INAzyme was immobilized in the microchannel of the microchip. Ampliflu Red instead of ABTS was chosen as the peroxidase substance for signaling due to its fast reaction kinetics and the strong fluorescence of its oxidized product resorufin, which would fulfill the continuous in vivo measurement requirements of fast acquisition speed and high sensitivity (Figure 6a).

The dynamic range of the platform was first evaluated. For the glucose concentrations from 100 to 1000 μM, a well-defined fluorescent response curve with a good linear relationship ($I(AU) = 297.1 + 2.936C_{glucose}/\mu M$, $R^2 = 0.95$) was obtained, revealing the feasibility for glucose quantification with the platform (Figure 6b). The platform's stability and reproducibility were then assessed. As depicted in Figure 6c, the fluorescent responses to 250 μM glucose remained almost unchanged during continuous monitoring over 1 h, suggesting the good stability of the platform for continuous measurement. Moreover, the platform exhibited almost negligible variations for repeated measurements (relative standard deviation = 4.8% for four measurements), indicating its excellent reproducibility (Figure 6d). The selectivity toward glucose measurement against potential interferences such as AA and lactate was also evaluated, demonstrating the capability of the platform for specific glucose monitoring (Figure S19).

The basal level of glucose in the striatum of living rat brains was first continuously monitored with the developed platform.

DOI: 10.1021/acs.analchem.6b00975
Anal. Chem. XXXX, XXX, XXX−XXX

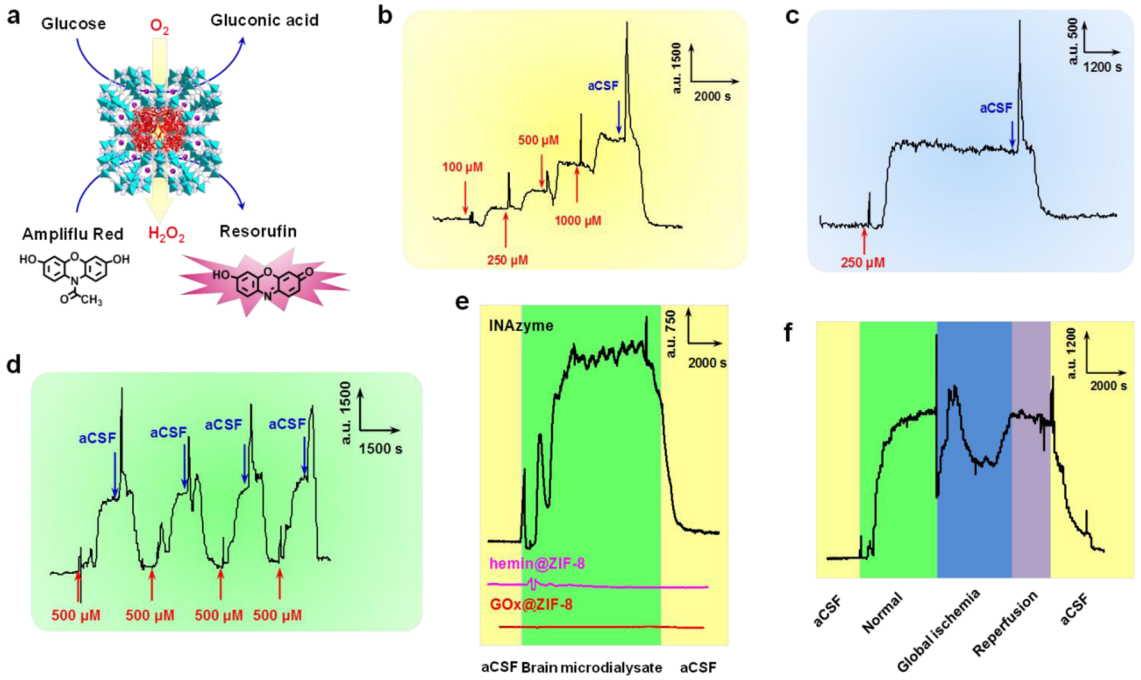

Figure 6. Continuous online measurements of cerebral glucose with the INAzyme-based integrative sensing platform. (a) Schematic illustration of the INAzyme-catalyzed cascade oxidation of glucose and nonfluorescent Ampliflu Red to produce fluorescent resorufin (λ_{ex} = 532 nm, λ_{em} = 585 nm). (b) Glucose concentration-dependent fluorescent intensity−time curve. The glucose concentrations ranged from 100 to 1000 μM. (c) Fluorescent intensity−time curve for 250 μM glucose over 1 h. (d) Fluorescent intensity−time curve for repeated measurement of 500 μM glucose for four times. (e) Continuously monitoring basal levels of glucose from the striatum of living rat brains on microfluidic chips modified with different nanomaterials (i.e., the INAzyme, hemin@ZIF-8, and GOx@ZIF-8). (f) Continuously monitoring the dynamic changes of glucose level in the striatum of a living rat brain following global ischemia/reperfusion with the INAzyme-based sensing platform.

As shown in Figure 6e, an apparent fluorescent response was observed when the sample was switched from aCSF to the microdialysate. The elevated fluorescent response could be ascribed to the cerebral glucose. The fluorescent response maintained at the elevated level during the continuous monitoring for more than 1 h, and the basal level of microdialysate glucose in the living rat striatum was measured to be 637.7 ± 19.2 μM (n = 3), which was consistent with the previously reported values.[58] To further ensure the elevated fluorescence was from microdialyzed glucose, hemin@ZIF-8 and GOx/ZIF-8 were immobilized on the microfluidic chips for measurements. For either case, no obviously elevated fluorescence was observed. These results demonstrated that the INAzyme-based platform could be successfully applied for the selectively in vivo monitoring cerebral glucose levels.

Since glucose plays a key role in brain energy metabolism and synaptic transmission and serves as a useful biomarker in acute human brain insults (e.g., stroke and head trauma), it is critically important to monitor its levels during ischemia stroke, one of the most fatal diseases in the world.[57] The dynamic change of striatum glucose level in the brains of living rats following global ischemia/reperfusion was then continuously monitored. As displayed in Figure 6f, the basal levels of striatum glucose were estimated to be 656.7 ± 20.3 μM (n = 3). When the rats were administrated with global ischemia, the glucose levels decreased to 49.1 ± 12.7% (n = 3) and then restored to 98.4 ± 10.1% (n = 3) of the basal level during the reperfusion process. The decrease in glucose levels after global ischemia measured with the integrative online platform was comparable to the values obtained with the off-line measurement above (50.2 ± 8.3% (n = 3), Figure 5c), establishing the capability of the INAzyme-based platform for effectively probing the dynamic variations of cerebral glucose associated with diseases/injuries with adequate temporal resolution in living animals.[59]

■ CONCLUSIONS

In summary, we have demonstrated a rational design for INAzymes with synergistically enhanced catalytic activity and remarkably improved stability as well as good recyclability, by exploring the nanoscale proximity effects. The INAzymes were formed by adaptively coassembling complementary catalytic guests within nanoscaled MOF matrixes. On the basis of the INAzyme-catalyzed cascade enzymatic reactions, both in vitro and in vivo glucose measurements have been achieved. Moreover, an integrative online sensing platform was developed by combining the INAzyme-modified microfluidic chip with microdialysis technology. With the established platform, the continuously monitoring the dynamic changes of cerebral glucose in living brains following ischemia/reperfusion was successfully illustrated. This study not only provides a facile strategy for synthesis of integrative nanozymes but also opens an innovative approach to developing platforms for in vivo analysis. Considering the vast combinations of available natural enzymes, artificial enzymes, and nanozymes, novel INAzymes are expected to be synthesized and integrated to the current platform for a wide range of targets associated with many critical diseases in other living animals and even human beings.

DOI: 10.1021/acs.analchem.6b00975
Anal. Chem. XXXX, XXX, XXX−XXX

■ ASSOCIATED CONTENT

Supporting Information

The Supporting Information is available free of charge on the ACS Publications website at DOI: 10.1021/acs.analchem.6b00975.

Additional experimental details, table of ζ-potentials, and figures with associated discussion (PDF)

■ AUTHOR INFORMATION

Corresponding Authors

*E-mail: zyzhou@nju.edu.cn.
*E-mail: xuejinzh@nju.edu.cn.
*E-mail: snie@emory.edu.
*E-mail: weihui@nju.edu.cn. Phone: +86-25-83593272. Fax: +86-25-83594648.

Author Contributions

The manuscript was written through contributions of all authors. All authors have given approval to the final version of the manuscript.

Notes

The authors declare no competing financial interest.

■ ACKNOWLEDGMENTS

This work was supported by NSFC (21405079, 21405081), NSF of Jiangsu Province (BK20130561), 973 Program (2015CB659400), PAPD program, Fundamental Research Funds for Central Universities (20620140617, 20620140627), Shuangchuang Program of Jiangsu Province, Six Talents Summit Program of Jiangsu Province, Open Funds of SKLEAC (SKLEAC201501), Open Funds of SKLACLS (SKLACLS1404), and Thousand Talents Program for Young Researchers. TEM and XRD experiments were carried out in part in the Engineering Joint Laboratory and Center of Modern Analysis at Nanjing University. The authors thank Professors Xinghua Xia and Kang Wang for microchip fabrication and Dr. Hang Xing for ZIF-8 model visualization.

■ REFERENCES

(1) Wei, H.; Wang, E. K. *Chem. Soc. Rev.* **2013**, *42*, 6060−6093.
(2) Wang, X. Y.; Hu, Y. H.; Wei, H. *Inorg. Chem. Front.* **2016**, *3*, 41−60.
(3) Gao, L. Z.; et al. *Nat. Nanotechnol.* **2007**, *2*, 577−583.
(4) Wei, H.; Wang, E. *Anal. Chem.* **2008**, *80*, 2250−2254.
(5) Liu, B. W.; Sun, Z. Y.; Huang, P. J. J.; Liu, J. W. *J. Am. Chem. Soc.* **2015**, *137*, 1290−1295.
(6) Asati, A.; Santra, S.; Kaittanis, C.; Nath, S.; Perez, J. M. *Angew. Chem., Int. Ed.* **2009**, *48*, 2308−2312.
(7) Zheng, X.; et al. *Angew. Chem., Int. Ed.* **2011**, *50*, 11994−11998.
(8) Ding, N.; Yan, N.; Ren, C. L.; Chen, X. G. *Anal. Chem.* **2010**, *82*, 5897−5899.
(9) Tang, Z. W.; Wu, H.; Zhang, Y. Y.; Li, Z. H.; Lin, Y. H. *Anal. Chem.* **2011**, *83*, 8611−8616.
(10) Wang, C. I.; Chen, W. T.; Chang, H. T. *Anal. Chem.* **2012**, *84*, 9706−9712.
(11) Ryabov, A. D.; Cerón-Camacho, R.; Saavedra-Díaz, O.; Denardo, M. A.; Ghosh, A.; Le Lagadec, R.; Collins, T. J. *Anal. Chem.* **2012**, *84*, 9096−9100.
(12) Xu, J.; Wu, J.; Zong, C.; Ju, H. X.; Yan, F. *Anal. Chem.* **2013**, *85*, 3374−3379.
(13) Zhang, L. N.; Deng, H. H.; Lin, F. L.; Xu, X. W.; Weng, S. H.; Liu, A. L.; Lin, X. H.; Xia, X. H.; Chen, W. *Anal. Chem.* **2014**, *86*, 2711−2718.
(14) Weerathunge, P.; Ramanathan, R.; Shukla, R.; Sharma, T. K.; Bansal, V. *Anal. Chem.* **2014**, *86*, 11937−11941.
(15) Wu, G. W.; He, S. B.; Peng, H. P.; Deng, H. H.; Liu, A. L.; Lin, X. H.; Xia, X. H.; Chen, W. *Anal. Chem.* **2014**, *86*, 10955−10960.
(16) Chen, S.; Hai, X.; Chen, X. W.; Wang, J. H. *Anal. Chem.* **2014**, *86*, 6689−6694.
(17) Jin, L. Y.; Dong, Y. M.; Wu, X. M.; Cao, G. X.; Wang, G. L. *Anal. Chem.* **2015**, *87*, 10429−10436.
(18) Gao, Z. Q.; Tang, D. Y.; Tang, D. P.; Niessner, R.; Knopp, D. *Anal. Chem.* **2015**, *87*, 10153−10160.
(19) Hizir, M. S.; Top, M.; Balcioglu, M.; Rana, M.; Robertson, N. M.; Shen, F. S.; Sheng, J.; Yigit, M. V. *Anal. Chem.* **2016**, *88*, 600−605.
(20) Zhao, Q.; Huang, H. W.; Zhang, L. Y.; Wang, L. Q.; Zeng, Y. L.; Xia, X. D.; Liu, F. P.; Chen, Y. *Anal. Chem.* **2016**, *88*, 1412−1418.
(21) Zhou, H.; Han, T.; Wei, Q.; Zhang, S. *Anal. Chem.* **2016**, *88*, 2976−2983.
(22) Guo, Y. J.; Deng, L.; Li, J.; Guo, S. J.; Wang, E. K.; Dong, S. J. *ACS Nano* **2011**, *5*, 1282−1290.
(23) Song, Y. J.; Qu, K. G.; Zhao, C.; Ren, J. S.; Qu, X. G. *Adv. Mater.* **2010**, *22*, 2206−2210.
(24) Liu, Y. L.; Zhao, X. J.; Yang, X. X.; Li, Y. F. *Analyst* **2013**, *138*, 4526−4531.
(25) Fan, K. L.; Cao, C. Q.; Pan, Y. X.; Lu, D.; Yang, D. L.; Feng, J.; Song, L. N.; Liang, M. M.; Yan, X. Y. *Nat. Nanotechnol.* **2012**, *7*, 459−464.
(26) Tonga, G. Y.; et al. *Nat. Chem.* **2015**, *7*, 597−603.
(27) Chen, J.; Patil, S.; Seal, S.; McGinnis, J. F. *Nat. Nanotechnol.* **2006**, *1*, 142−150.
(28) Xue, T.; Peng, B.; Xue, M.; Zhong, X.; Chiu, C.-Y.; Yang, S.; Qu, Y.; Ruan, L.; Jiang, S.; Dubin, S.; Kaner, R. B.; Zink, J. I.; Meyerhoff, M. E.; Duan, X.; Huang, Y. *Nat. Commun.* **2014**, *5*, 3200.
(29) Vernekar, A. A.; Sinha, D.; Srivastava, S.; Paramasivam, P. U.; D'Silva, P.; Mugesh, G. *Nat. Commun.* **2014**, *5*, 5301.
(30) Kim, C. K.; et al. *Angew. Chem., Int. Ed.* **2012**, *51*, 11039−11043.
(31) Zhang, Y.; Wang, Z.; Li, X.; Wang, L.; Yin, M.; Wang, L.; Chen, N.; Fan, C.; Song, H. *Adv. Mater.* **2016**, *28*, 1387−1393.
(32) Karakoti, A. S.; Singh, S.; Kumar, A.; Malinska, M.; Kuchibhatla, S.; Wozniak, K.; Self, W. T.; Seal, S. *J. Am. Chem. Soc.* **2009**, *131*, 14144−14145.
(33) Diez-Castellnou, M.; Mancin, F.; Scrimin, P. *J. Am. Chem. Soc.* **2014**, *136*, 1158−1161.
(34) Larsen, R. W.; Wojtas, L.; Perman, J.; Musselman, R. L.; Zaworotko, M. J.; Vetromile, C. M. *J. Am. Chem. Soc.* **2011**, *133*, 10356−10359.
(35) Liu, Y.; et al. *J. Am. Chem. Soc.* **2015**, *137*, 14952−14958.
(36) Manea, F.; Houillon, F. B.; Pasquato, L.; Scrimin, P. *Angew. Chem., Int. Ed.* **2004**, *43*, 6165−6169.
(37) Li, Y. Y.; et al. *Angew. Chem., Int. Ed.* **2015**, *54*, 1832−1835.
(38) Lin, Y. H.; Wu, L.; Huang, Y. Y.; Ren, J. S.; Qu, X. G. *Chem. Sci.* **2015**, *6*, 1272−1276.
(39) Wang, L. H.; Zeng, Y.; Shen, A. G.; Zhou, X. D.; Hu, J. M. *Chem. Commun.* **2015**, *51*, 2052−2055.
(40) Pandey, P.; Singh, J.; Achary, V. M.; Reddy, M. K. *Front. Envrion. Sci.* **2015**, *3*, 00025.
(41) Liu, Y.; et al. *Nat. Nanotechnol.* **2013**, *8*, 187−192.
(42) Zhao, Z.; Fu, J.; Dhakal, S.; Johnson-Buck, A.; Liu, M.; Zhang, T.; Woodbury, N. W.; Liu, Y.; Walter, N. G.; Yan, H. *Nat. Commun.* **2016**, *7*, 10619.
(43) Engstrom, K.; Johnston, E. V.; Verho, O.; Gustafson, K. P. J.; Shakeri, M.; Tai, C. W.; Backvall, J. E. *Angew. Chem., Int. Ed.* **2013**, *52*, 14006−14010.
(44) Lu, G.; Li, S.; Guo, Z.; Farha, O. K.; Hauser, B. G.; Qi, X.; Wang, Y.; Wang, X.; Han, S.; Liu, X.; DuChene, J. S.; Zhang, H.; Zhang, Q.; Chen, X.; Ma, J.; Loo, S. C.; Wei, W. D.; Yang, Y.; Hupp, J. T.; Huo, F. *Nat. Chem.* **2012**, *4*, 310−316.
(45) Furukawa, H.; Cordova, K. E.; O'Keeffe, M.; Yaghi, O. M. *Science* **2013**, *341*, 974.
(46) Mao, Y. Y.; Li, J. W.; Cao, W.; Ying, Y. L.; Hu, P.; Liu, Y.; Sun, L. W.; Wang, H. T.; Jin, C. H.; Peng, X. S. *Nat. Commun.* **2014**, *5*, 5532.

DOI: 10.1021/acs.analchem.6b00975
Anal. Chem. XXXX, XXX, XXX−XXX

(47) (a) Shieh, F. K.; et al. *J. Am. Chem. Soc.* **2015**, *137*, 4276−4279. (b) Liang, K.; et al. *Nat. Commun.* **2015**, *6*, 7240. (c) Liu, X.; He, L.; Zheng, J.; Guo, J.; Bi, F.; Ma, X.; Zhao, K.; Liu, Y.; Song, R.; Tang, Z. *Adv. Mater.* **2015**, *27*, 3273−3277.
(48) Liang, H.; Jiang, S. H.; Yuan, Q. P.; Li, G. F.; Wang, F.; Zhang, Z. J.; Liu, J. W. *Nanoscale* **2016**, *8*, 6071−6078.
(49) Wei, H.; Li, B. L.; Du, Y.; Dong, S. J.; Wang, E. K. *Chem. Mater.* **2007**, *19*, 2987−2993.
(50) He, M.; Yao, J.; Liu, Q.; Wang, K.; Chen, F.; Wang, H. *Microporous Mesoporous Mater.* **2014**, *184*, 55−60.
(51) Cheng, H. J.; Wang, X. Y.; Wei, H. *Anal. Chem.* **2015**, *87*, 8889−8895.
(52) Cheng, H.; Qiu, X.; Zhao, X.; Meng, W.; Huo, D.; Wei, H. *Anal. Chem.* **2016**, *88*, 2937−2943.
(53) Lin, Y.; Zhu, N.; Yu, P.; Su, L.; Mao, L. *Anal. Chem.* **2009**, *81*, 2067−2074.
(54) Zhang, L.; Han, Y.; Zhao, F.; Shi, G.; Tian, Y. *Anal. Chem.* **2015**, *87*, 2931−2936.
(55) Phan, A.; Doonan, C. J.; Uribe-Romo, F. J.; Knobler, C. B.; O'keeffe, M.; Yaghi, O. M. *Acc. Chem. Res.* **2010**, *43*, 58−67.
(56) Travascio, P.; Li, Y.; Sen, D. *Chem. Biol.* **1998**, *5*, 505−517.
(57) Rossi, D. J.; Brady, J. D.; Mohr, C. *Nat. Neurosci.* **2007**, *10*, 1377−1386.
(58) Zhuang, X.; Wang, D.; Lin, Y.; Yang, L.; Yu, P.; Jiang, W.; Mao, L. *Anal. Chem.* **2012**, *84*, 1900−1906.
(59) Brody, D. L.; Magnoni, S.; Schwetye, K. E.; Spinner, M. L.; Esparza, T. J.; Stocchetti, N.; Zipfel, G. J.; Holtzman, D. M. *Science* **2008**, *321*, 1221−1224.

DOI: 10.1021/acs.analchem.6b00975
Anal. Chem. XXXX, XXX, XXX−XXX